Raman excitation profile of the G band in single-chirality carbon nanotubes

Raman excitation profile of the *G* band in single-chirality carbon nanotubes

L. G. Moura,[1,2] M. V. O. Moutinho,[3] P. Venezuela,[3] C. Fantini,[1] A. Righi,[1] M. S. Strano,[4] and M. A. Pimenta[1]

[1]*Departamento de Física, Universidade Federal de Minas Gerais, Belo Horizonte, Brazil*

[2]*Departamento de Física, Universidade Federal de Viçosa, Viçosa, Brazil*

[3]*Instituto de Física, Universidade Federal Fluminense, 24210-346 Niterói, RJ, Brazil*

[4]*Department of Chemical Engineering, Massachusetts Institute of Technology, Cambridge, Massachusetts 02139, USA*

(Received 8 October 2013; published 6 January 2014)

We present in this work measurements of the Raman excitation profile of the high-energy phonons (*G* band) in single-chirality (n,m) semiconducting single-wall carbon nanotubes using more than 70 laser excitation energies, and a theoretical description based on the third-order quantum model for Raman scattering. We show that the observed asymmetry in the *G* band Raman excitation profile is rigorously explained by considering all physical elements associated with Raman scattering in (n,m) carbon nanotubes, such as the existence of van Hove singularities in the electronic density of states and wave-vector dependence of the matrix elements of the Raman process. We conclude that the proposed violation of the Condon approximation is not a fundamental principle underlying the nanotube photophysics.

DOI: 10.1103/PhysRevB.89.035402 PACS number(s): 78.67.Ch, 61.48.De, 78.30.Jw, 78.30.Na

I. INTRODUCTION

Raman spectroscopy is one of the most important experimental techniques used to study the physical properties of graphene and carbon nanotubes [1,2]. The Raman signal of carbon nanotubes is hugely enhanced when the laser energy is in resonance with optical transitions associated with the van Hove singularities in the nanotube density of states [3]. Despite the fact that the Raman excitation profile (REP) of the *G* band in nanotube bundles [4] and of the radial breathing modes (RBMs) in single-chirality (n,m) nanotubes [5,6] have been studied for many years, only recently was the excitation profile of the high-energy phonons (*G* band) of specific single-chirality (n,m) nanotubes experimentally determined [7,8]. In these previous works [7,8], the observed REP asymmetry could only be explained in the framework the semiclassical second-order model for Raman scattering considering two discrete electronic levels, leading those authors to propose that the asymmetry was a manifestation of the violation of the Condon approximation in carbon nanotubes. We will present in this work measurements of the *G* band of single-chirality (n,m) nanotubes as a function of the laser energy and the explanation for the *G*-band excitation profile based on the fundamental principles of Raman scattering [9,10], considering all physical ingredients for the determination of Raman intensities in carbon nanotubes.

In the Raman spectrum of a single-wall carbon nanotube (SWNT), the band associated with the low-energy radial breathing modes (RBMs) appears in the range 100–400 cm^{-1}, and its frequency is inversely proportional to the nanotube diameter [5]. The RBM Raman excitation profile of individual (n,m) nanotubes can be obtained even in samples containing mixed nanotube species, since the RBM peak of each (n,m) nanotube can be spectrally distinguished. The RBM Raman excitation map provides structural (n,m) characterization of the nanotube species present in the sample [5,6]. However, the frequencies of high-energy phonons (*G* band) are weakly dependent on the nanotube (n,m) chirality, preventing the measurement of *G*-band REP of a specific (n,m) nanotube in samples containing many different (n,m) nanotube species. Measurements of the *G*-band REP of individual (n,m) nanotubes were performed only recently [7], after it became possible to produce samples containing enriched species of specific (n,m) nanotubes.

In this work, we present measurements of the REPs of the *G* band of the (6,5) and (7,5) nanotubes using more than 70 laser excitation lines. Our results are interpreted within the framework of the quantum-field third-order model for Raman scattering, showing that the observed REP asymmetry is ascribed, in part, to the presence of van Hove singularities in the joint density of electronic transitions in carbon nanotubes and also by the wave-vector dependence of the matrix elements of the Raman-scattering process in carbon nanotubes. We conclude that the use of the semiclassical second-order model within the non-Condon approximation is not needed to describe Raman intensities in carbon nanotubes.

II. EXPERIMENTAL DETAILS

Chirality-enriched carbon nanotube samples were prepared by the linear density gradient ultracentrifugation (DGU) method, using the procedure described in Ref. [11]. All measurements were performed from liquid phase nanotube dispersions, and the spectrum of cyclohexane was used as a reference for the frequencies and intensities calibration. The experiments were performed at room temperature using a Dilor XY triple spectrometer and using several different laser lines of a tunable dye laser (DCM Special, Rhodamine R6G, and Rhodamine R560 dyes), covering the range 662–542 nm, with steps of 2 or 3 nm, and the laser lines 530.9, 520.8, 514.5, 501.7, 496.5, and 488.0 nm of an Ar/Kr ion laser. The laser power focused on the samples ranged from 1 to 15 mW, and the position and width of the Raman peaks remained practically independent of the laser power.

III. RESULTS

Figure 1(a) shows the Raman spectrum of the sample, recorded with the 585 nm (2.12 eV) laser line, where we can observe the RBM peaks between 300 and 350 cm^{-1}, the

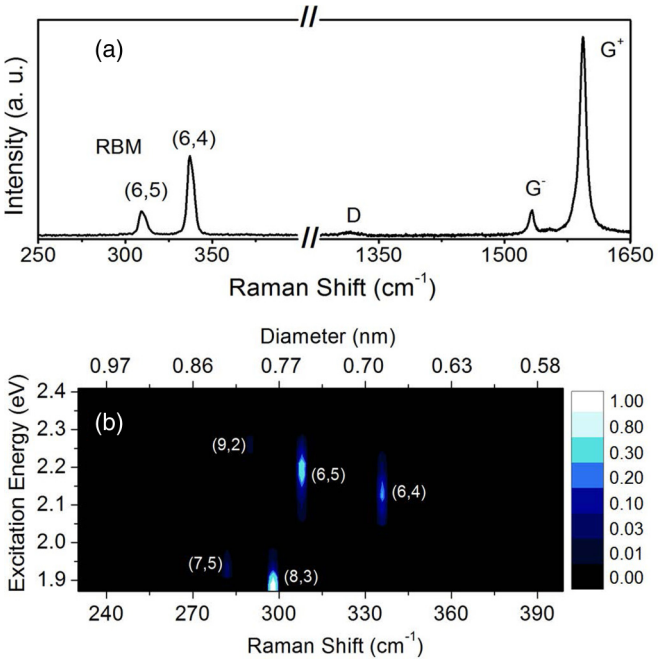

FIG. 1. (Color online) (a) Raman spectra sample recorded with the 585 nm (2.12 eV) laser line, showing the most important spectral features: RBM, D, and G bands. (b) Resonance Raman maps of RBM bands obtained with different excitation energies, revealing the existence of nanotubes with different chiralities in the sample.

D band around 1300 cm^{-1}, and the G band in the range 1500–1600 cm^{-1}. The G band is split into two prominent peaks, centered around 1528 and 1590 cm^{-1}, assigned as G^- and G^+, and associated, respectively, with the TO (transverse-optical) and LO (longitudinal-optical) phonon modes of semiconducting nanotubes [1].

Figure 1(b) shows the REP map of the RBMs, where each spot is associated with a specific (n,m) nanotube present in the sample. The bottom horizontal scale represents the Raman frequency and it is related to the upper scale by the equation $d = 219/(\omega_{\mathrm{RBM}} - 15)$, where ω_{RBM} is the RBM frequency in cm^{-1} and d is the nanotube diameter in nm [5]. The vertical axis represents the laser excitation energies used in the experiments, and the color scale represents the normalized intensities of the Raman signal.

Figure 2(a) shows the G-band spectra obtained with up to 70 different laser excitation energies. Figures 2(b) and 2(c) show the experimental REP of the (6,5) nanotube RBM peak and of the G^- peak at 1528 cm^{-1}, respectively. The RBM REP cannot be resolved into two peaks, associated with resonances with incoming and outgoing photons, due to the small RBM phonon energy compared to the width of the resonance profile. On the other hand, Fig. 2(c) clearly shows the two maxima in the REP of the G^- peak. Comparing the incoming resonance maxima in Figs. 2(b) and 2(c), we conclude that the G^- peak at 1528 cm^{-1} is associated with the (6,5) nanotube.

We can observe in Fig. 2(c) that the REP of the G band is asymmetric, since its two maxima have different intensities. The lower-energy maximum (incoming resonance) is more intense than the higher-energy one (outgoing resonance), and the same kind of behavior was observed for the other G-band components of different (n,m) nanotubes studied in this work. The asymmetry in the G-band REP was also observed in previous works for other (n,m) nanotube species [7,8]. Those authors analyzed this result using the semiclassical second-order model for Raman intensities, and they proposed that this asymmetry was a manifestation of the violation of the Condon approximation in nanotubes. We will show in the following that the quantum-field model can precisely describe the Raman intensities of all Raman features in nanotubes.

IV. DISCUSSION

Let us first discuss the semiclassical second-order model for Raman intensities [12]. This model is based on the quantum nature of the electronic polarizability, but the electric field of the radiation is treated classically. Within this approximation, Raman scattering corresponds to a second-order process involving only two optical transitions (absorption of the incident photon and emission of the scattered one). In this case, the quantum process associated with the creation (or destruction) of quanta of vibrational energy is not considered explicitly [10]. The semiclassical model has been very useful to explain Raman intensities in molecules [13,14], and provides the most common picture to represent the Raman scattering process.

Within the semiclassical second-order approximation, the theoretical expression for Raman intensities is based on the Kramers-Heisenberg dispersion equation, through

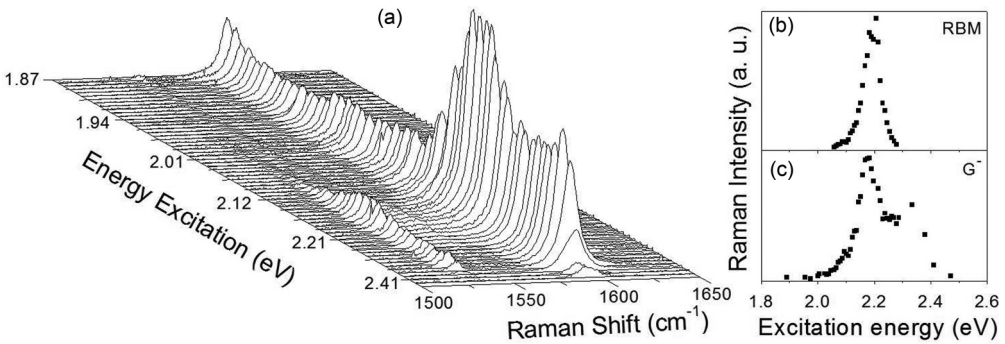

FIG. 2. The G-band spectra obtained with 70 different excitation energies. (b) Raman excitation profile (intensity versus laser energy) of the RBM peak at 308 cm^{-1} associated with the (6,5) nanotube. (c) Raman excitation profile of the G^- peak at 1528 cm^{-1}.

second-order time-dependent perturbation theory [12], and is given by

$$I(E_L) = K \left| \sum_{|a\rangle} \frac{\langle f|H_{e\text{-}r}|a\rangle\langle a|H_{e\text{-}r}|i\rangle}{(E_L - E_a - i\gamma)} \right|^2, \quad (1)$$

where E_L is the laser energy, $|i\rangle$, $|f\rangle$, and $|a\rangle$ correspond, respectively, to the initial, final, and intermediate states, E_a is the energy of the intermediate state $|a\rangle$, $H_{e\text{-}r}$ is the electron-radiation Hamiltonian, and γ is a damping constant related to the finite lifetime τ of the intermediate state $|a\rangle$. The sum in Eq. (1) is taken over all possible intermediate states $|a\rangle$.

A correction in the semiclassical model can be introduced afterward by expanding the electronic polarizability as a Taylor series in terms of the vibrational normal coordinates [12]. Far from resonances, the zeroth- and first-order terms of this expansion give rise, respectively, to the Rayleigh and Raman scattering. However, near resonances, both the zeroth- and first-order terms generate Raman scattering, and they are related to the so-called A and B Albrecht terms (in fact, A''' and B''' in Albrecht's original paper [12]). Since the Condon approximation states that the electronic transition moments are independent of the nuclear coordinates, the A and B Albrecht terms are associated, respectively, with the Condon (coordinate-independent) and non-Condon (coordinate-dependent) processes [13].

Since the semiclassical expression given in Eq. (1) contains only one term in the denominator, resonances with incident and scattered photons only occur if we consider different electronic and vibrational states in the sum of Eq. (1), such as in the case of the so-called four-level model, in which we consider only two electronic levels (ground and excited states) and two vibrational levels ($v = 0$ and 1) [7]. Considering the four-level model, the semiclassical expression given in Eq. (1) reduces to [7]

$$I(E_L) = K \left| \frac{1 + C}{(E_L - E_{00'} - i\gamma)} - \frac{1 - C}{(E_L - E_{01'} - i\gamma)} \right|^2. \quad (2)$$

In this approximation, resonances with incident and scattered photons are associated with the minima of the two denominators on the right-hand side of Eq. (2). The constant C is directly related with the matrix elements involving the first-order (non-Condon) term in the Taylor expansion of the electronic transition dipole operator [7]. Non-null values of C give rise to the different intensities of the two maxima in the REP, associated with incoming and outgoing resonances, respectively. Therefore, within the context of the semiclassical approximation for Raman intensities, an asymmetric REP can be considered as a signature of a non-Condon process [7,8].

The G-band REP of single-chirality nanotubes was fit in Refs. [7] and [8] considering a non-null value for the constant C, leading the authors to suggest that the REP asymmetry was a manifestation of the violation of the Condon approximation and associated with the molecular nature of the atomic vibrations in carbon nanotubes. We will show in the following that the G-band REP asymmetry data can be well described by the third-order quantum model, which provides a fundamental understanding of Raman scattering in both molecules and condensed-matter systems.

If we consider only two discrete electronic levels, the third-order description of Raman scattering predicts a symmetric REP, where the maxima associated with the incoming and outgoing resonances have the same intensities. This approximation was used to describe the REP of nanotubes in bundles [4] and of the RBM of single-chirality nanotubes [5], but it cannot describe the asymmetric G-band profile of single-chirality nanotubes. However, as shown below, the asymmetry occurs when we consider the electronic band structure of a carbon nanotube and the k dependence of the electron-photon and electron-phonon matrix elements.

Within the third-order quantum-field model for Raman scattering and in the framework of perturbation theory, the G-band intensity is calculated as

$$I_G(E_L) = E_L(E_L - \hbar\omega_G)^3 \left| \frac{1}{N_k} \sum_{\mathbf{k}} \frac{\langle \mathbf{k}\pi|D_{\text{out}}|\mathbf{k}\pi^*\rangle\langle \mathbf{k}\pi^*|\Delta H_G|\mathbf{k}\pi^*\rangle\langle \mathbf{k}\pi^*|D_{\text{in}}|\mathbf{k}\pi\rangle}{[E_L - E_{\pi\pi^*}(\mathbf{k}) - \hbar\omega_G - i\gamma][E_L - E_{\pi\pi^*}(\mathbf{k}) - i\gamma]} \right|^2, \quad (3)$$

where $|\mathbf{k}\pi\rangle$ and $|\mathbf{k}\pi^*\rangle$ are the electronic states in the valence and conduction bands, respectively, $D_{\text{in(out)}}$ is the operator coupling the incident (scattered) photons with the electrons of the material, and ΔH_G is the electron-phonon coupling operator. Explicit expressions for electron-photon and electron-phonon matrix elements can be found in Ref. [15]. The broadening energy γ is the inverse of the electronic lifetime and $E_{\pi\pi^*}(\mathbf{k}) = E_{\pi^*}(\mathbf{k}) - E_{\pi}(\mathbf{k})$ is the energetic separation between valence and conduction electronic eigenstates. The resonance conditions are then achieved when $E_L = E_{\pi^*}(\mathbf{k}) - E_{\pi}(\mathbf{k})$ or $E_L = E_{\pi^*}(\mathbf{k}) - E_{\pi}(\mathbf{k}) + \hbar\omega_G$.

When the phonon belongs to the totally symmetric irreducible representation, the two terms in the denominator of Eq. (3) give rise to resonances with incident and scattered photons, respectively (incoming and outgoing resonances) [5]. Notice that this is an intrinsic characteristic of a third-order process, contrary to the case of the semiclassical second-order process, in which resonances with incident and scattered photons only appear when we consider approximations such as the four-level model used in Refs. [7] and [8] and shown in Eq. (2).

The electronic structure, $E_\alpha(\mathbf{k})$ and $|\mathbf{k}\alpha\rangle$ with $\alpha = \pi,\pi^*$, is obtained from *ab initio* calculations fitted to a tight-binding (TB) model up to fifth neighbors with one orbital per site [15]. The G-band normal modes are described taking in account the correct symmetry of the specific nanotube. The electronic structure of an (n,m) carbon nanotube is obtained by zone folding the graphene ones. As $\mathbf{K_1}$ and $\mathbf{K_2}$ are the reciprocal-lattice vectors along the circumferential direction and the nanotube axis, respectively,

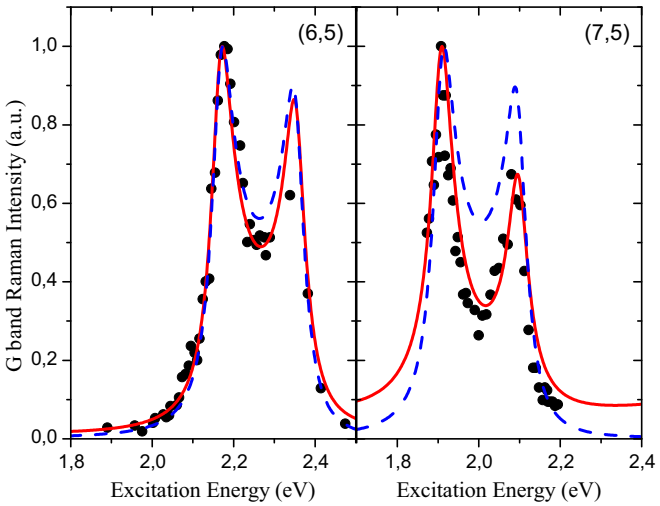

FIG. 3. (Color online) G-band REP for (6,5) and (7,5) carbon nanotubes. The black circles are experimental data and the full red line is the present calculation with all matrix elements, while the dashed blue line is the same calculation using constant matrix elements. The electronic gap between the valence and conduction bands was corrected in a few electronvolts to fit with the experimental transitions.

we have

$$E_{\alpha\mu}(k) = E_{\alpha}^{2D}\left(k\frac{\mathbf{K_2}}{|\mathbf{K_2}|} + \mu\mathbf{K_1}\right), \tag{4}$$

where $\mu = 0, \ldots, N-1$, $-\pi/T < k < \pi/T$, and

$$\mathbf{K_1} = \frac{1}{N}(-t_2\mathbf{b_1} + t_1\mathbf{b_2}), \quad \mathbf{K_2} = \frac{1}{N}(m\mathbf{b_1} - n\mathbf{b_2}), \tag{5}$$

where N is the number of hexagons in the nanotube unit cell, $\mathbf{T} = t_1\mathbf{a_1} + t_2\mathbf{a_2}$ is the translational vector, and $(\mathbf{b_1},\mathbf{b_2})$ are the graphene reciprocal-lattice vectors.

We can replace the sum over $\mathbf{k}$ in Eq. (3) by sums over μ and k using the reciprocal-lattice vectors $\mathbf{K_1}$ and $\mathbf{K_2}$ to obtain the G-band Raman intensity for a specific nanotube under some restrictions: the light, in the electron-photon matrix elements, must be polarized along the nanotube axis, i.e., $\vec{P}_{\rm in} = \vec{P}_{\rm out} \propto \mathbf{T}$, and the G-band phonon eigenvectors need to be adjusted for the particular nanotube chirality. For the G-band frequency ω_G, the experimental value is taken and the broadening energy is $\gamma = 25$ meV.

Figure 3 shows the calculated G-band Raman intensity as a function of excitation energy for (6,5) and (7,5) carbon nanotubes. Solid lines are the results of the full calculation described above, and dashed lines are the calculations considering constant matrix elements in Eq. (3). It is interesting to notice that the calculations with constant matrix elements reproduce qualitatively the measured asymmetry between the two maxima in the REP. Thus the asymmetry is primarily due to the density of states of the nanotube. The inclusion of the correct matrix elements in the calculation further improves the agreement with the experimental data, showing that the wave-vector dependence of the matrix elements is also an important ingredient to describe the G-band intensity in carbon nanotubes.

Although we did not include explicitly the excitonic effects in our calculations, they are partially taken into account, since we consider many-body effects in the electronic structure (which increases the electronic band gap), and we decrease the separation E_{22}^S transition between the second van Hove singularities in the valence and conduction bands to account for the exciton binding energy.

It was shown by Duque *et al.* [8] that the quantum interference between different E_{ii}^S transitions also gives rise to REP asymmetry. In the case of the (n,m) nanotubes studied in this work, this kind of quantum interference is negligible, because the first, third, and fourth excitonic transitions of these nanotubes are far below or above the range of laser energies used in our work. We thus conclude that REP asymmetry is an intrinsic characteristic Raman scattering in carbon nanotubes.

V. CONCLUSION

In summary, we presented in this work resonant Raman measurements in chirality-enriched samples of carbon nanotubes using many different laser lines, which allowed us to obtain the Raman excitation profiles (REPs) of the G band in the single-chirality nanotubes. We have demonstrated that the G-band intensities and the REP asymmetry can be well described by the third-order quantum model by considering all physical ingredients relevant for the Raman scattering process in nanotubes, such as the electronic structure of the nanotubes and the matrix elements of the Raman process. Our results show that the proposed violation of the Condon approximation [7,8] is not a fundamental issue in the photophysics of a carbon nanotube, and it is just a consequence of considering the dependence of the electronic polarizability on the nuclear coordinates within the second-order semiclassical approximation for Raman scattering. This dependence is an expected result when considering the strong electron-phonon interaction in carbon nanotubes [2]. Our conclusions also call into question the proposed statement of the molecular nature of vibrations in nanotubes [7], which would be useful for an understanding of the bridge between the worlds of molecular chemistry and solid-state physics [7], and they demonstrate that the third-order quantum-field model always provides a correct description of Raman intensities in both molecules and condensed-matter systems [10].

ACKNOWLEDGMENTS

This work was supported by the Brazilian Nanocarbon Institute of Science and Technology (INCT/Nanocarbono), the Brazilian Network on Carbon Nanotube Research, and the Brazilian agencies CNPq, CAPES, and FAPEMIG.

[1] R. Saito, C. Fantini, and J. Jiang, Top. Appl. Phys. **111**, 251 (2008).

[2] L. M. Malard, M. A. Pimenta, G. Dresselhaus, and M. S. Dresselhaus, Phys. Rep. **473**, 51 (2009).

[3] A. M. Rao, E. Richter, S. Bandow, B. Chase, P. C. Eklund, K. A. Williams, S. Fang, K. R. Subbaswamy, M. Menon, A. Thess, R. E. Smalley, G. Dresselhaus, and M. S. Dresselhaus, Science **275**, 187 (1997)

[4] M. A. Pimenta, A. Marucci, S. A. Empedocles, M. G. Bawendi, E. B. Hanlon, A. M. Rao, P. C. Eklund, R. E. Smalley, G. Dresselhaus, and M. S. Dresselhaus, Phys. Rev. B **58**, R16016 (1998).

[5] C. Fantini, A. Jorio, M. Souza, M. S. Strano, M. S. Dresselhaus, and M. A. Pimenta, Phys. Rev. Lett. **93**, 147406 (2004).

[6] H. Telg, J. Maultzsch, S. Reich, F. Hennrich, and C. Thomsen, Phys. Rev. Lett. **93**, 177401 (2004).

[7] J. G. Duque, H. Chen, A. K. Swan, A. P. Shreve, S. Kilina, S. Tretiak, X. Tu, M. Zheng, and S. K. Doorn, ACS Nano **5**, 5233 (2011).

[8] J. G. Duque, H. Telg, H. Chen, A. K. Swan, A. P. Shreve, X. Tu, M. Zheng, and S. K. Doorn, Phys. Rev. Lett. **108**, 117404 (2012).

[9] R. Loudon, Proc. R. Soc. London, Ser. A **275**, 218 (1963).

[10] W. L. Peticolas, L. Napie, P. Stein, and B. Fanconi, J. Chem. Phys. **52**, 1576 (1970).

[11] M. S. Arnold, A. A. Green, J. F. Hulvat, S. I. Stupp, and M. C. Hersam, Nat. Nano. **1**, 60 (2006).

[12] A. C. Albrecht, J. Chem. Phys. **34**, 1476 (1961).

[13] R. Kumble, J. Phys. Chem. B **102**, 7280 (1998).

[14] R. He, N. G. Tassi, G. B. Blanchet, and A. Pinczuk, Phys. Rev. B **83**, 115452 (2011).

[15] P. Venezuela, M. Lazzeri, and F. Mauri, Phys. Rev. B **84**, 035433 (2011).